Simulation of Heat and Mass Transfer Processes in Elements of a Sodium-Cooled Reactor Circuit

Ulugbek Noraliyev[1,2, a)], Kalibek Shamsiyev[1], Ikromjon Umarov[1], Khasan Umarvayev[1], Yayra Mukhiddinova[1]

[1]*Tashkent state technical university named after Islam Karimov, Tashkent, Uzbekistan*
[2]*Termez State University of Engineering and Agrotechnologies, Termez, Uzbekistan*

[a)] *Corresponding author: noraliyevulugbek@gmail.com*

Abstract. This study focuses on the simulation of heat and mass transfer processes in the circuit elements of a sodium-cooled fast reactor, specifically testing the LOGOS software package on a benchmark problem involving thermal mixing in a T-junction from the Phenix reactor. The work includes a review of computational fluid dynamics (CFD) methods such as Reynolds-Averaged Navier-Stokes (RANS), Large Eddy Simulation (LES), and Direct Numerical Simulation (DNS). Numerical modeling in LOGOS was performed using three grid resolutions, with results compared to experimental data. Key findings indicate good agreement between simulated and experimental temperature profiles, with relative deviations not exceeding -0.3% ±2% on the finest grid. The study highlights the suitability of LOGOS for modeling thermal-hydraulic processes in liquid-metal-cooled reactors, emphasizing safety implications related to thermal fatigue.

INTRODUCTION

Sodium exhibits favorable properties for nuclear power reactors, including high heat transfer capacity and a wide temperature range between its melting point (371 K) and boiling point (1155 K) at atmospheric pressure. However, sodium is highly flammable, igniting upon contact with air oxygen at operational temperatures, producing dense white smoke composed of sodium oxides (Na_2O and Na_2O_2) that react with humidity to form caustic sodium hydroxide (NaOH) and subsequently carbonate (Na_2CO_3) [1]. Sodium fires from leaks can cause significant structural damage, as observed in the 1986 Almeria solar power plant incident [1]. Historical sodium leaks in reactors range from grams to about 2 tons [2], often due to flow-induced vibrations (e.g., Monju reactor in December 1995 [3,4]) or thermal fatigue (e.g., Superphenix in April 1990).

Thermal fatigue arises from mixing flows at different temperatures, leading to fluctuating temperature fields in the fluid, which transfer to adjacent structures with minimal attenuation due to sodium's high heat transfer coefficient [10,11]. In liquid-metal fast reactors (LMFRs), potential thermal striping occurs in the upper plenum from mixing jets of fuel, breeder, and control assemblies, as well as in T-junctions in primary (loop-type reactors), secondary, and auxiliary circuits [10,11]. To mitigate sodium leak risks from thermal fatigue or vibrations, detailed thermal-hydraulic analyses for steady and transient states are essential [12,13]. CFD codes are employed for such calculations, with flows in T-junctions simulated using RANS [14,15], LES [16,19], and DNS [20,21].

This paper examines RANS and LES approaches for sodium flow in the Phenix reactor's T-junction configuration, where an upstream elbow induces skewed velocity distribution, flow separation, and secondary flows [22,24]. Results from RANS simulations are presented, focusing on coarse and fine grids with wall refinement. LES results emphasize wall temperature fluctuations and thermal fatigue zones. Additionally, the LOGOS software is tested for modeling these processes, comparing simulations to experimental data.

Historical and Operational Context of the Phenix Reactor. The Phenix prototype sodium-cooled fast breeder reactor, located in Marcoule, France, began construction in November 1968, achieved first divergence in August 1973, and grid connection in December 1973, reaching 580 MWth (260 MWe) in March 1974 [2]. It operated with a closed fuel cycle from 1979, achieving a breeding ratio of 1.16. Over 30 years, it provided operational experience for fast neutron reactors and supported R&D for Generation IV systems. Phenix featured a tank-type design with

core, three primary pumps, six intermediate heat exchangers, and one rotating plug . The vessel held 800 tons of sodium under 40 mbar argon cover gas. Sodium entered at 380°C and exited at 530°C. The 1.5 m diameter, 0.85 m high core used (U-Pu)O_2 fuel with 23-28% plutonium in hexagonal stainless steel-clad assemblies.

Phenix demonstrated self-stabilizing thermal feedbacks, low spatial effects, and high thermal inertia for safety margins. No high pressure or phase changes in the primary circuit; no boron for reactivity compensation, avoiding xenon poisoning. Four automatic scrams in the 1990s due to negative reactivity transients were hypothesized as sodium bubble explosions [2].

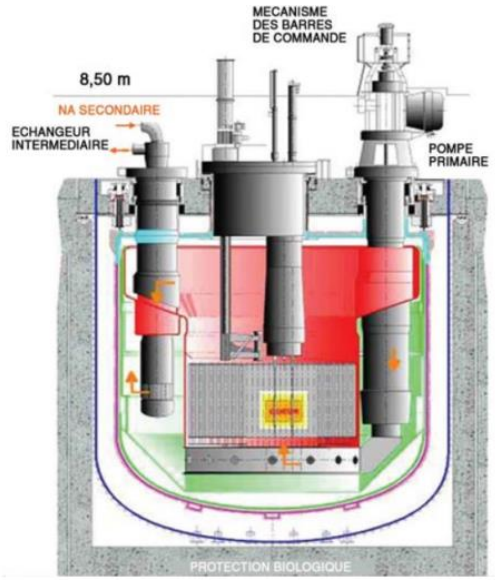

FIGURE 1. Reactor section

Phenix demonstrated self-stabilizing thermal feedbacks, low spatial effects, and high thermal inertia for safety margins. No high pressure or phase changes in the primary circuit; no boron for reactivity compensation, avoiding xenon poisoning. Four automatic scrams in the 1990s due to negative reactivity transients were hypothesized as sodium bubble explosions [2].

TABLE 1. Assignment of the phases in the slots

Problem Area / Component	**Contribution to Downtime**
Intermediate Heat Exchangers	26.91 %
Scheduled Maintenance	14.72 %
Steam Generators	13.46 %
Fuel Reloading	11.99 %
Negative Reactivity Insertions	7.92 %
Turbogenerator and its Systems	7.02 %
Fuel Assemblies	2.93 %
Secondary Circuit	2.54 %
Control Systems	2.34 %
Sodium Leaks	2.54 %
Personnel Errors	0.29 %
Other	7.34 %

Construction used a continuous metal lining for the underground reactor compartment, with 10 mm thick horizontal and 5 mm vertical sheets. Lifetime electricity production: 24,440.402 GWh, with availability factors of 45.81% (energy), 39.91% (load), 41% (capacity). Downtime causes listed in Table 1, including heat exchanger leaks and four A.U.R.N. incidents in 1989-1990 from reactivity spikes, possibly due to assembly expansion [2].Predecessor: Rapsodie (40 MWth, 1967-1983). Successor: Superphenix (3000 MWth, 1985-1998, closed politically). Future: ASTRID in 2020s.

EXPERIMENTAL RESEARCH

Approaches to Thermal-Hydraulic Modeling in Reactors.

CFD is a modern tool for verifying engineering designs by computing flow characteristics using physico-mathematical methods. It enables assessment of system performance and external influences before detailed design, testing hypotheses and concepts. Experiments and CFD simulations bridge knowledge gaps, with CFD increasingly relied upon due to the high cost and difficulty of experiments, especially for local effects not captured by system codes. In LMFRs, wire wraps as spacers for fuel rods require detailed local flow knowledge [5,6].

Coolant flow exiting the core comprises outlets from various fuel assemblies heated to different temperatures, causing temperature fluctuations that may lead to thermal fatigue in structures [7]. Accurate characterization of liquid metal flow structure above the core is crucial. This section reviews modeling methods for heat and mass transfer in fuel assemblies and plenum hydraulics in LMFRs, emphasizing CFD developments, particularly by the Nuclear Research and Consultancy Group (NRG) in the Netherlands [7].

Nuclear phenomena span system (plant-wide), component (specific part), and meso (small part) scales. Codes: System (RELAP, TRACE) for transients; subchannel (COBRA-TF, VIPRE) for local parameters; porous (CUPID); CFD (ANSYS-CFX) for detailed flows [26,27]. Multi-scale coupling integrates these [29], addressing 1D limitations with 3D effects.:

Computational Fluid Dynamics (CFD):

For innovative nuclear systems' coolants, experiments are expensive and measurements challenging, making CFD an attractive complement for predicting flow characteristics. CFD solves the fundamental fluid physics equations discretely on computers, capturing flow evolution in detail. For laminar flows with low Reynolds numbers, equations can be solved directly. Turbulent flows are more complex.

Advantages of CFD include comprehensive domain analysis and enhanced result visualization. Real experiments struggle with measuring wind direction, pollutant concentration, chemical reactions, and radiation. CFD applications in energy include predicting NOx, SOx, and solid formation; slag on heating surfaces; surface temperature optimization; abrasion-prone area identification; design verification; efficient air distribution; cost reduction via computer testing; and product testing speed.

Direct Numerical Simulation (DNS):

DNS, popular among researchers despite high resource costs, uses the finest grid to resolve smallest eddy structures, providing detailed flow visualization and accounting for turbulent eddy thermal energy. Turbulence is nonlinear with broad spatial and temporal scales; large scales depend on geometry and boundaries, small on flow itself. DNS resolves all relevant scales, increasing in realism with computing power, but not expected for practical nuclear engineering soon [8]. Smallest scales estimated from Kolmogorov theory: the Kolmogorov length scale.

$$\eta = \left(\frac{\nu^3}{\varepsilon}\right)^{0.25} \quad (1)$$

DNS, popular among researchers despite high resource costs, uses the finest grid to resolve smallest eddy structures, providing detailed flow visualization and accounting for turbulent eddy thermal energy. Turbulence is nonlinear with broad spatial and temporal scales; large scales depend on geometry and boundaries, small on flow itself. DNS resolves all relevant scales, increasing in realism with computing power, but not expected for practical nuclear engineering soon [8]. Smallest scales estimated from Kolmogorov theory: the Kolmogorov length scale.

Large Eddy Simulation (LES):

LES resolves large eddies in unsteady formulations using filtered equations, excluding subgrid eddies. Subgrid turbulence models (e.g., Smagorinsky) approximate small eddies. Implicit LES (ILES) uses numerical dissipation without explicit models, proposed by Belotserkovsky [25]. Detached Eddy Simulation (DES) combines RANS for boundary layers and LES elsewhere, addressing coarse LES grids' inability to resolve wall layers [25].

LES advantages: Resolves eddy structures in detail, though costlier (more cells, smaller time steps). It computes losses from turbulent regime, potentially universal for isotropic flows where macroscopic features dominate large eddies. Limited to simple geometries due to high resource demands; uses high-order spatial discretization for broader turbulence scales.

Reynolds-Averaged Navier-Stokes (RANS)

RANS uses Reynolds equations, decomposing instantaneous parameters into mean and fluctuating components. Equations are unclosed, leading to various turbulence models (one- or multi-parameter). Most CFD packages include RANS, making it common in engineering. Models lack universality, developed for specific task classes over decades.

Investigation of Heat and Mass Transfer in the Phenix Reactor

Phenix, built from 1968-1973 in Marcoule, France, achieved 580 MWth with a closed fuel cycle and breeding ratio 1.16 [2]. It supported Generation IV R&D and waste transmutation. Operated by French (80%) and Italian (20%) entities, it produced 24,440 GWh with availabilities around 40-45%.

RESEARCH RESULTS

Numerical Modeling of Sodium Mixing in Phenix T-Junction

The Phenix secondary circuit T-junction features a horizontal straight section, 90° elbow (radius 762 mm, thickness 9.35 mm), and vertical straight with branch pipe (inner diameter 68 mm, thickness 2.5 mm) . Main pipe: inner diameter 494 mm, thickness 7 mm. Normal operation: main sodium at 613 K, flow 800 kg/s ($Re \approx 6 \times 10^6$); branch at 703 K, 7 kg/s ($Re \approx 5 \times 10^5$), ΔT = 90 K.

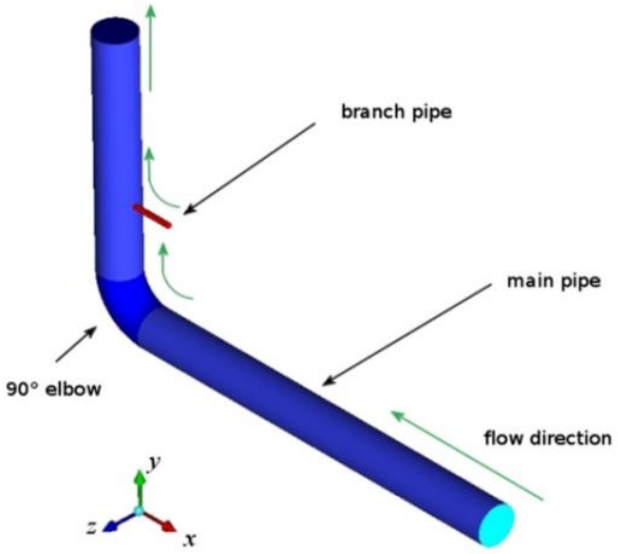

FIGURE 2. Schematic diagram of the T-junction in the "Fenix" secondary circuit

CFD modeling used Fluent with second-order implicit time-stepping, upwind convection, and SIMPLE pressure-velocity coupling. RANS used Reynolds Stress Model (RSM); LES used Wall-Adapting Local Eddy-Viscosity (WALE) with Pr _t = 0.85. Boundaries: outlet convection pressure, adiabatic walls. Inlet turbulence via vortex method.

Three RANS grids: 0.5M cells (wall law), 3.5M cells (no-slip), 4.8M cells (conjugate heat transfer). LES on 4.8M grid.

RANS Results

Inlet conditions compared: constant velocity, developed profiles. Selected developed profile for realism. Momentum ratio

$$MR = \frac{(\rho_m U_m^2 D_m^2)}{(\rho_b U_b^2 D_b^2)} = 42 \quad (2)$$

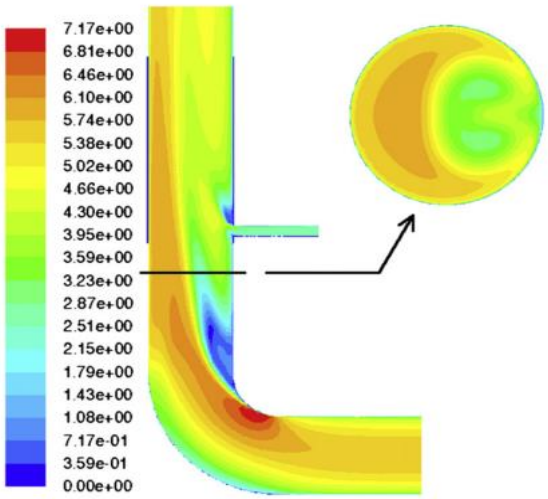

FIGURE 3. Mean velocity (m/s) in the T-junction for RANS simulation

Indicates reattaching jet. Upstream elbow skews velocity

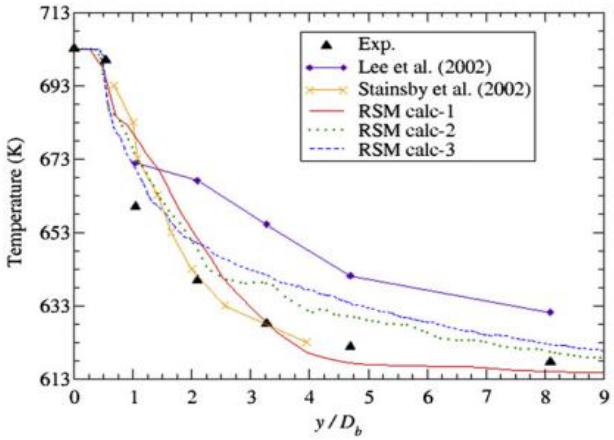

FIGURE 4. Mean temperature from RANS calculations along the main pipe wall outside the branch connection.

Temperature profiles along wall downstream of branch show fine grid and no-slip improving agreement, though overprediction >3 Db. Conjugate heat transfer smooths profiles.

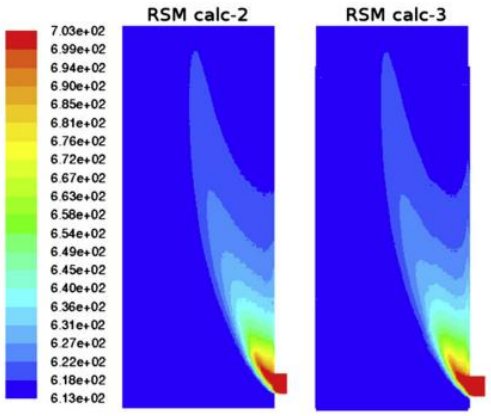

FIGURE 5. Temperature profiles (K) downstream of the hot branch in RSM Calc-2 (without wall conduction) and RSM Calc-3 (conjugate heat transfer) models

Temperature contours show mixing zone to y/Db ≈16 center, y/Db ≈10 near wall.

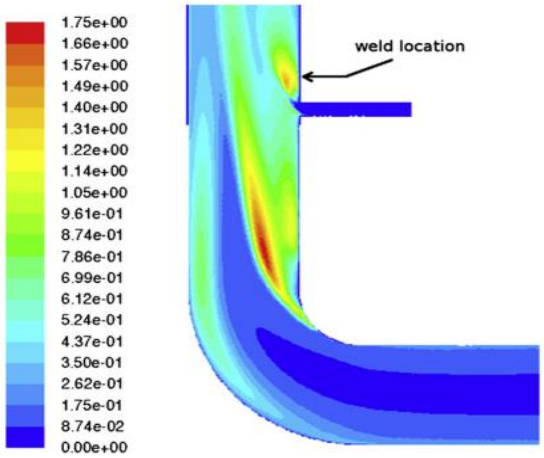

FIGURE 6. Turbulent kinetic energy (m²/s²) in the RSM Calc-3 simulation.

Turbulent kinetic energy peaks at shear layer and mixing zone, linking to fatigue cracks

LES Results

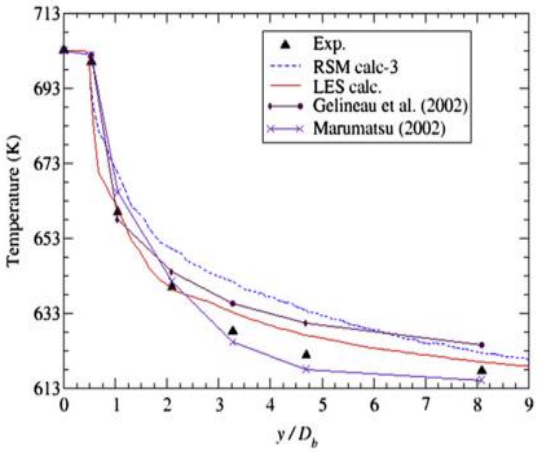

FIGURE 7. Mean temperature from LES results along the main pipe wall downstream of the branch.

LES captures reattaching jet, better matching experimental temperature profiles, especially near inlet.

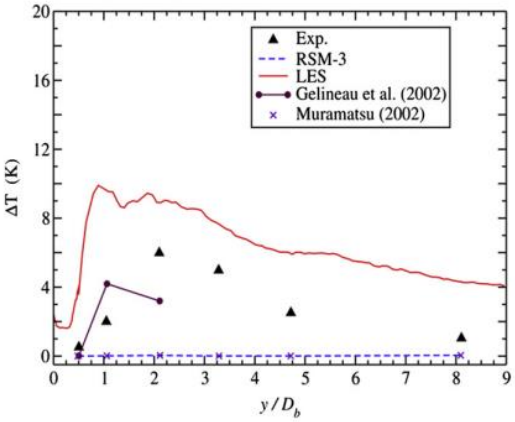

FIGURE 8. Peak-to-peak temperature difference on the outer surface of the main pipe casing.

Peak-to-peak fluctuations agree well.

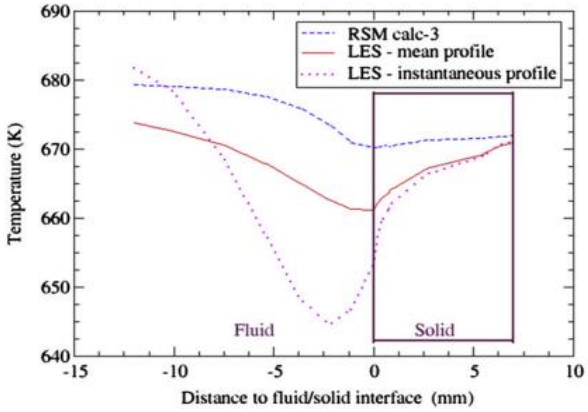

FIGURE 9. Temperature profiles at the liquid/solid interface

Interface temperature profiles show higher gradients than RANS.

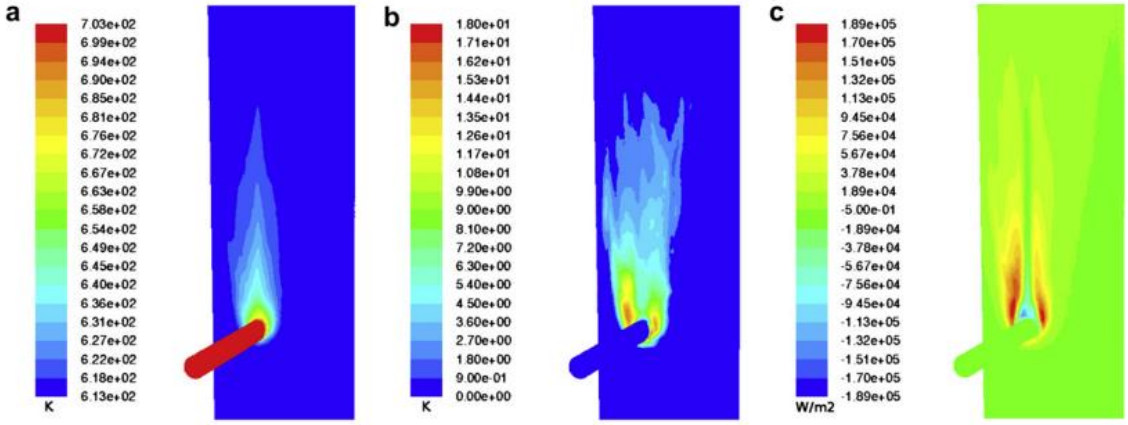

FIGURE 10. Contours of (a) mean temperature, (b) root mean square temperature, and (c) mean surface heat flux at the liquid/solid interface.

Contours of mean temperature, RMS, and heat flux identify hot spot and high-fluctuation plume matching experimental white/black spots and crack locations.

Modeling Mixing of Sodium Flows in LOGOS Software and Comparison with Experimental Data

Problem Setup.

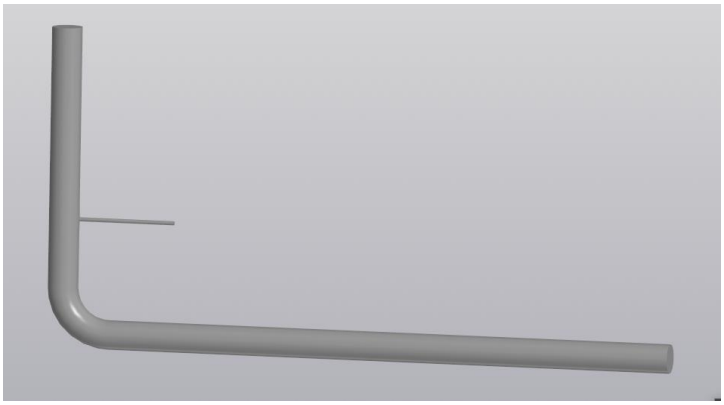

FIGURE 11. Geometric model of the computational domain.

Geometric model built in KOMPAS-3D: main pipe 494 mm diameter with 90° elbow (radius 762 mm), branch 68 mm at 2600 mm from elbow. Imported to LOGOS for gridding.

TABLE 2. Mesh Parameters

Grid No.	Base Cell Size	Number of Elements	Number of Nodes
1	0.005	8,116,470	8,969,468
2	0.01	2,040,227	2,245,039
3	0.02	747,255	936,569

Boundary/initial conditions

TABLE 3. Calculation Parameters, Boundary and Initial Conditions

No.	**Parameter**	**Value**
1	Turbulence Model	Reynolds Stress Model (RSM)
2	Sodium Flow Rate at Main Pipe Inlet, kg/s	800
3	Sodium Temperature at Main Pipe Inlet, K	613
4	Boundary Condition on Lateral Surfaces	No-slip and Thermal Insulation
5	Outlet Boundary Condition	Pressure Outlet (Subsonic)
6	Sodium Flow Rate at Branch Inlet, kg/s	7
7	Sodium Temperature at Branch Inlet, K	703

Simulation Results

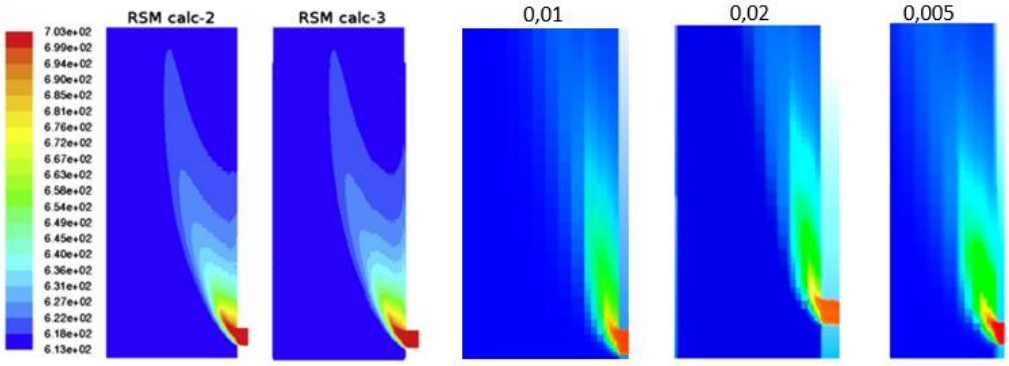

FIGURE 12. Temperature (K) fields in the computational domain

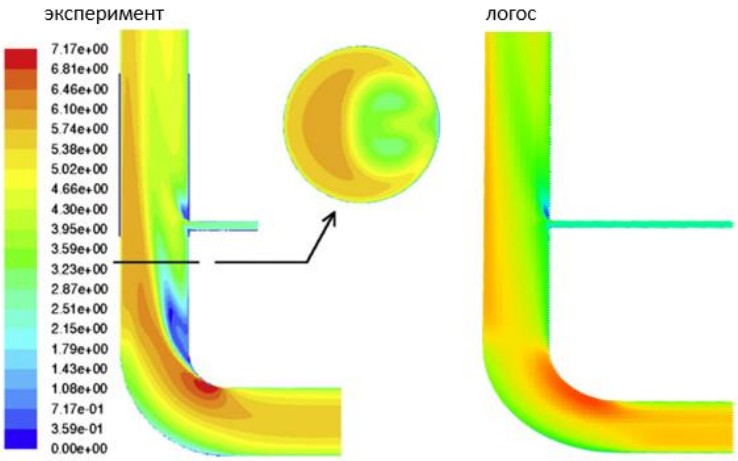

FIGURE 13. Velocity fields

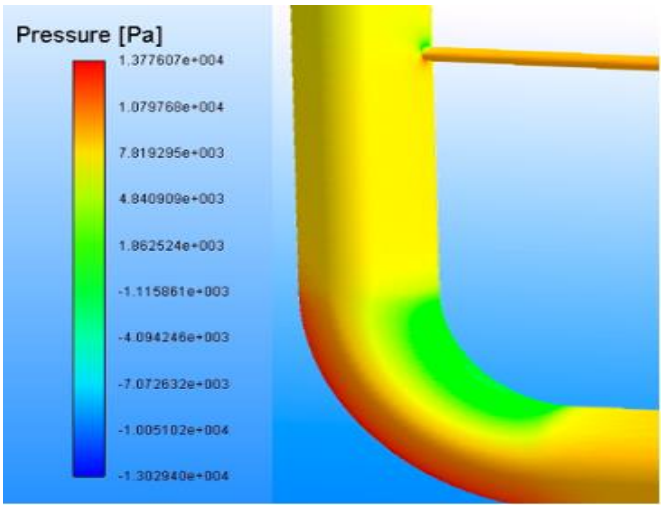

FIGURE 14. Pressure field in the computational domain

LOGOS yielded temperature velocity, and pressure fields.

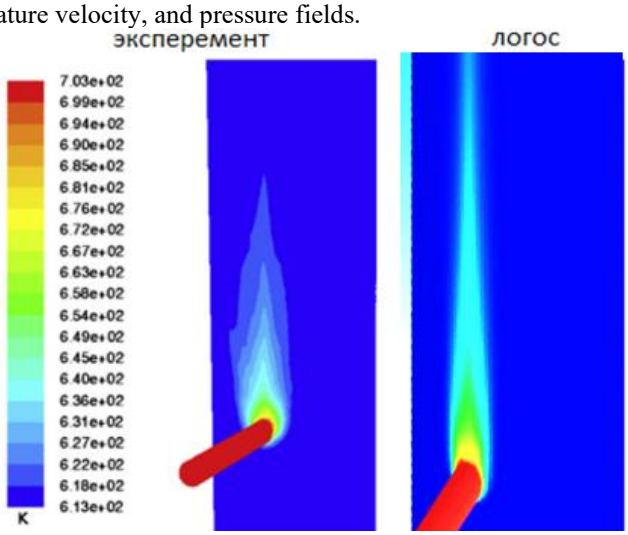

FIGURE 15. Sodium temperature field near the pipe surface

Near-wall temperature near T-junction.

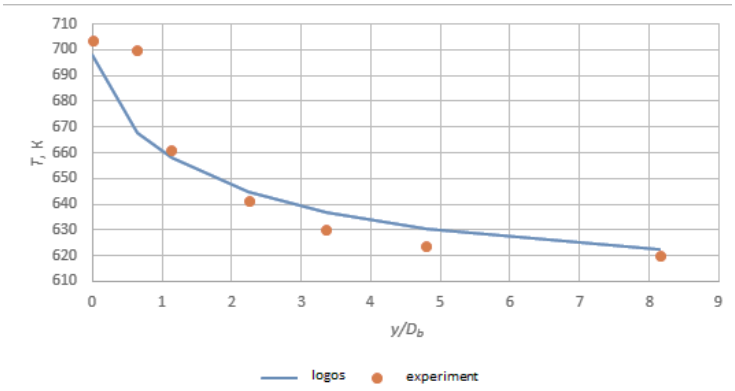

FIGURE 16. Temperature profile along the thermal wake for Grid #1

Profiles along thermal wake compared to experiments

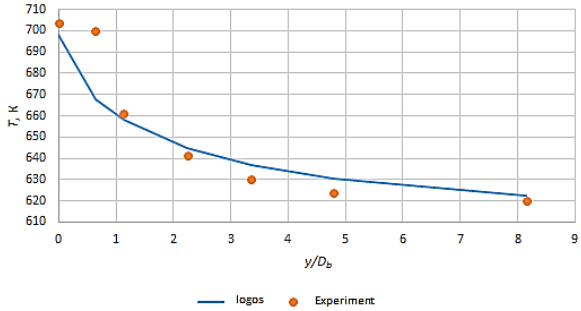

FIGURE 17. Temperature profile along the thermal wake for Grid 2,

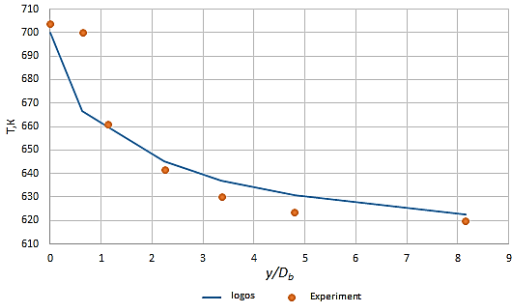

FIGURE 18. Temperature profile along the thermal wake for Grid 3

TABLE 4. Comparison of Simulation Results with Experimental Data

y/Db	T exp	Grid 1	Grid 2	Grid 3
0.000	703.933	698.078	701.169	700.000
0.637	700.200	667.561	688.414	666.800
1.132	661.000	657.907	669.848	659.900
2.246	641.533	644.584	653.673	645.000
3.360	630.067	636.780	645.947	636.900
4.792	623.667	630.515	638.578	630.747
8.151	619.933	622.517	628.091	622.500

Statistical analysis: Relative deviation

$$\mathrm{E}_n = \frac{(S_n - D_n)}{D*} \tag{3}$$

where D* is maximum experimental temperature difference. Mean and standard deviation

TABLE 5. Statistical Analysis Results

	y/Db	Grid 1	Grid 2	Grid 3
E_n	0.000	-0.00832	-0.00393	-0.00560
	0.637	-0.04661	-0.01683	-0.04770
	1.132	-0.00468	0.01339	-0.00170
	2.246	0.00476	0.01892	0.00541
	3.360	0.01066	0.02520	0.01085
	4.792	0.01098	0.02391	0.01136
	8.151	0.00417	0.01316	0.00414
$\bar{E}$		-0.00296	0.01055	-0.00331
u_E		0.02003	0.01548	0.02052

Profiles match qualitatively, with initial steeper drop in LOGOS, but good overall agreement

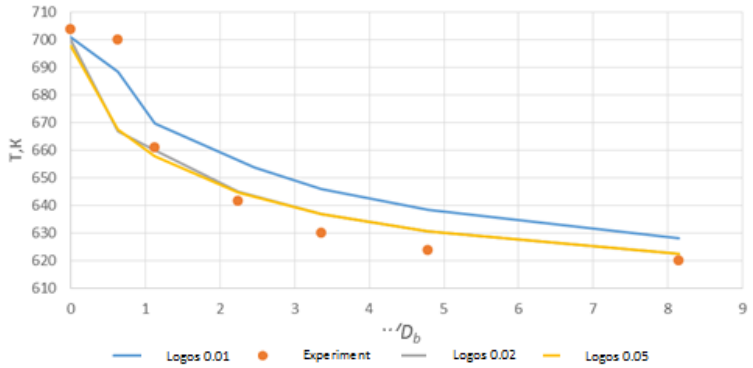

FIGURE 19. Comparison of calculated temperature profiles with experimental data

CONCLUSIONS

RANS provides efficient initial estimates but underpredicts fluctuations; LES better captures dynamics for fatigue assessment. LOGOS demonstrates capability for sodium mixing simulations, with grid-independent results supporting its use in LMFR design. Conjugate heat transfer essential for accurate wall predictions. Findings align with Phenix incidents, emphasizing CFD for safety. This work tested LOGOS on Phenix T-junction mixing, achieving good experimental agreement. LOGOS is suitable for heat-mass transfer modeling in sodium-cooled reactor circuits.

REFERENCES

1. V. P. Luster, K. F. Freudenstein, Feedback from practical experience with large sodium fire accidents, in: Technical Committee Meeting on Evaluation of Radioactive Materials Release and Sodium Fires in Fast Reactors, O-aria, Ibaraki, Japan, 1996. J. Guidez, L. Martin, S. C. Chetal, P. Chellapandi, B. Raj, Lessons learned from sodium-cooled fast reactor operation and their ramifications for future reactors with respect to enhanced safety and reliability, Nucl. Technol. 164 (2) (2008) 207–220. DOI: 10.13182/NT08-A4012
2. F. Roelofs, V. R. Gopala, S. Jayaraju, A. Shams, E. Komen, Review of fuel assembly and pool thermal hydraulics for fast reactors, Nucl. Eng. Des. 265 (2013) 1205–1222. DOI: 10.1016/j.nucengdes.2013.07.018
3. M. Kondo, Y. Anoda, Water flow simulation test on flow-induced oscillation of thermowell in prototype fast breeder reactor monju: flow-induced vibration of bluff bodies, JSME Int. J. Ser. B. Fluids Therm. Eng. 44 (4) (2001) 688–694. DOI: 10.1299/jsmeb.44.688
4. IAEA, Fast Reactor Database, 2006 Update, IAEA-TECDOC-1531, Vienna, Austria. H. Aït Abderrahim, P. Kupschus, E. Malambu, Ph. Benoit, K. Van Tichelen, B. Arien, F. Vermeersch, P. D'hondt, Y. Jongen, S. Ternier, D. Vandeplassche, MYRRHA: A multipurpose accelerator driven system for research & development, Nucl. Instrum. Methods Phys. Res. A 463 (3) (2001) 487–494. DOI: 10.1016/S0168-9002(01)00167-2 (Note: 2010 reference likely relates to project updates; original MYRRHA paper cited)
5. F. Roelofs, V. R. Gopala, S. Jayaraju, A. Shams, E. Komen, Review of fuel assembly and pool thermal hydraulics for fast reactors, Nucl. Eng. Des. 265 (2013) 1205–1222. DOI: 10.1016/j.nucengdes.2013.07.018
6. P. Moin, K. Mahesh, Direct numerical simulation: a tool in turbulence research, Annu. Rev. Fluid Mech. 30 (1998) 539–578. DOI: 10.1146/annurev.fluid.30.1.539
7. G. Grötzbach, Challenges in low-Prandtl number heat transfer simulation and modelling, Nucl. Eng. Des. 237 (5) (2007) 462–474. DOI: 10.1016/j.nucengdes.2006.08.003
8. S. Chapuliot, C. Gourdin, T. Payen, J. P. Magnaud, A. Monavon, Hydro-thermal-mechanical analysis of thermal fatigue in a mixing tee, Nucl. Eng. Des. 235 (5) (2005) 575–596. DOI: 10.1016/j.nucengdes.2004.08.052
9. J. I. Lee, L. Hu, P. Saha, M. S. Kazimi, Numerical analysis of thermal striping induced high cycle thermal fatigue in a mixing tee, Nucl. Eng. Des. 239 (5) (2009) 833–839. DOI: 10.1016/j.nucengdes.2008.12.025
10. G. Grötzbach, M. Wörner, Direct numerical and large eddy simulations in nuclear applications, Int. J. Heat Fluid Flow 20 (3) (1999) 222–240. DOI: 10.1016/S0142-727X(99)00012-0
11. J.-P. Simoneau, J. Champigny, O. Gelineau, Applications of large eddy simulations in nuclear field, Nucl. Eng. Des. 240 (2) (2010) 429–439. DOI: 10.1016/j.nucengdes.2009.09.035

12. T. Frank, C. Lifante, H.-M. Prasser, F. Menter, Simulation of turbulent and thermal mixing in T-junctions using URANS and scale-resolving turbulence models in ANSYS CFX, Nucl. Eng. Des. 240 (9) (2010) 2313–2328. DOI: 10.1016/j.nucengdes.2009.11.023
13. E. Merzari, H. Ninokata, E. Baglietto, Large Eddy Simulation of the Flow in a T-junction, in: ICAPP 2009, Tokyo, Japan, 2009, Paper 9463.
14. Tee Junction - Comparison of Temperature Fluctuations with Experiments, in: 5th International Conference on Nuclear Engineering, Nice, France, 1997, ICONES-2145.
15. P. Coste, P. Quemere, P. Roubin, P. Emonot, M. Tanaka, H. Kamide, Large Eddy Simulation of a Mixing-T Experiment, in: ICAPP 2006, Reno, USA, 2006, pp. 1626–1635.
16. L. Meyer, Measurements of turbulent velocity and temperature in axial flow through a heated rod bundle, Nucl. Eng. Des. 146 (1-3) (1994) 71–82. DOI: 10.1016/0029-5493(94)90321-2
17. M. Tanaka, H. Ohshima, H. Monji, Numerical simulation of thermal striping phenomena in a T-junction piping system using large eddy simulation, J. Power Ener. Sys. 3 (1) (2009) 237–248. DOI: 10.1299/jpes.3.237
18. N. Fukushima, K. Fukagata, N. Kasagi, H. Noguchi, K. Tanimoto, Numerical and Experimental Study on Turbulent Thermal Mixing in a T-Junction Flow, in: The 6th ASME-JSME Thermal Engineering Joint Conference, Hawaii, USA, 2003, TED-AJ03-582.
19. I. Tiselj, R. Bergant, B. Mavko, I. Bajsic, G. Hetsroni, DNS of turbulent heat transfer in channel flow with heat conduction in the solid wall, J. Heat Transfer 123 (5) (2001) 849–857. DOI: 10.1115/1.1389465
20. M. Igarashi, N. Tanaka, M. Kimura, H. Kamide, Study on Fluid Temperature Fluctuation and Transfer to Wall in a Mixing Tee, in: 11th ICONE, Tokyo, Japan, 2003, 36299. R. Meyder, Turbulent velocity and temperature distribution in the central subchannel of rod bundles, Nucl. Eng. Des. 35 (2) (1975) 181–189. DOI: 10.1016/0029-5493(75)90196-X
21. N. Kimura, H. Ogawa, H. Kamide, Experimental study on fluid mixing phenomena in T-pipe junction with upstream elbow, Nucl. Eng. Des. 240 (10) (2010) 3055–3066. DOI: 10.1016/j.nucengdes.2010.05.027
22. P. R. Spalart, M. Shur, M. Strelets, Initial noise predictions for rudimentary landing gear as a workshop on benchmark problems for airframe noise computations-I, in: 29th AIAA Aeroacoustics Conference, Vancouver, Canada, 2008. DOI: 10.2514/6.2011-2769
23. A. Moorthi, A. Sharma, B. K. Velusamy, A review of sub-channel thermal hydraulic codes for nuclear reactor core and future directions, Nucl. Eng. Des. 335 (2018) 241–257. DOI: 10.1016/j.nucengdes.2018.03.012
24. J. Mahaffy, B. Chung, F. Dubois, F. Ducros, E. Graffard, M. Heitsch, M. Henriksson, T. Hohne, F. Menter, F. Moretti, P. Muhlbauer, P. Rohde, M. Scheuerer, B. L. Smith, T. Watanabe, C. Zigh, Best Practice Guidelines for the Use of CFD in Nuclear Reactor Safety Applications, OECD/NEA Report NEA/CSNI/R(2007)5, 2007.
25. Y. H. Ho, C. H. Lin, C. Pan, CFD modeling of full vessel upper plenum in Maanshan Nuclear Power Plant, Nucl. Eng. Des. 249 (2012) 175–181. DOI: 10.1016/j.nucengdes.2012.03.041 (Representative example from 2010s)
26. S. Kliem, A. Grahn, T. Höhne, T. V. Dinh, M. Scheuerer, The NURESAFE European Project: Advanced Numerical Simulation and Modelling for Reactor Safety, in: Proceedings of NENE 2015, Portorož, Slovenia, 2015.